Prediction of Transient Slab Temperature Distribution in the Re-heating Furnace of a Walking-beam Type for Rolling of Steel Slabs

Jong Gyu KIM and Kang Y. HUH[1]

Graduate student, Department of Mechanical Engineering, Pohang University of Science & Technology, Pohang, Kyungbuk 790-784, Korea.   1) Department of Mechanical Engineering, Pohang University of Science & Technology, Pohang, Kyungbuk 790-784, Korea. E-mail: huh@postech.ac.kr.

This article is on heat transfer analysis by the commercial code, FLUENT, for slabs heated in a walking-beam type of a re-heating furnace in POSCO (Pohang Iron & Steel Co., Ltd.). Steady state, three-dimensional analysis is performed for turbulent reactive flow and radiative heat transfer in the furnace. Computation is based on the Favre-averaged conservation equations of mass, momentum, energy and species with the k–ε turbulence model. The predicted global energy flow is in good agreement with the measurement. Two-dimensional transient calculation is performed for conduction in a slab with the boundary condition given in terms of the calculated local heat flux in the furnace. Results show substantial variation of the temperature across the furnace as well as between skid and non-skid regions in the slab. Parametric study is performed to examine skid mark severity and energy loss to the skid system with respect to the height and shape of the skid button and the convective heat transfer coefficient to cooling water. It is shown that the radiative exposure, which depends on the height and shape of the skid button, reduces skid mark severity by decreasing heat loss from the slab. The convective heat transfer coefficient to the cooling water turns out not to be of as much significance to skid mark severity as the exposure area of the skid button.

KEY WORDS: re-heating furnace; slab; skid mark severity; radiative exposure.

1. Introduction

Heating efficiency, skid marks, scale formation and emission of the pollutants such as NOx and soot are the major issues in design and operation of a re-heating furnace for hot rolling of steel slabs. There are two different methods of moving slabs in a re-heating furnace—a pusher type and a walking beam type. Slabs are moved by a pusher while supported by a skid system in the pusher type. On the other hand slabs are moved by walking beams while supported by fixed beams in the walking beam type. The fixed beams include the skid system composed of skid buttons, insulation and skid pipes. The rolling load and quality of the final products are determined by the degree of non-uniform temperature distribution in the slabs, primarily due to non-uniform heat flux and skid marks at contact points. The non-uniform heat flux depends on locations and types of burners, supply conditions of fuel and combustion air and geometry of the furnace chamber. Skid marks are generated by heat loss from the slabs through the skid system, eventually to cooling water.

Ford et al.[1] presented the heat transfer model for a steel slab and a water-cooled skid pipe in a multi-zone furnace. They provided the soaking times required to limit the temperature gradient in the slab within 55 K/m. Heat transfer to cooling water could be reduced due to a higher inlet temperature of the cooling water. Zongyu Li et al.[2] calculated the radiative exchange in a furnace chamber by the zone method.[3] They obtained the transient thermal response of a slab by finite difference approximation. Barr[4] developed the steady state heat transfer model for a pusher type of a re-heating furnace. He applied the zone method for radiative heat transfer and performed two-dimensional conduction calculation in a steel slab and a skid system. Three-dimensional analysis was recently performed by Kim et al.[5] with FLUENT[6] for turbulent reactive flow and heat transfer in a walking beam type of a re-heating furnace. To determine the overall heat transfer coefficient measurements were also made for the rising temperatures at different locations in the slabs.

2. Mathematical Models

2.1. Conservation Equations

The Favre-averaged continuity, momentum and energy equations can be written in the Cartesian coordinate as,

$$\frac{\partial \bar{\rho}}{\partial t} + \frac{\partial \bar{\rho} \tilde{u}_i}{\partial x_i} = 0 \quad ....(1)$$

$$\frac{\partial \bar{\rho}\tilde{u}_i}{\partial t} + \frac{\partial \bar{\rho}\tilde{u}_i \tilde{u}_j}{\partial x_j} = \frac{\partial}{\partial x_j}\left[\mu\left(\frac{\partial \tilde{u}_i}{\partial x_j} + \frac{\partial \tilde{u}_j}{\partial x_i}\right) - \left(\frac{2}{3}\mu\frac{\partial \tilde{u}_l}{\partial x_l}\right)\right]$$

$$-\frac{\partial \bar{p}}{\partial x_i} + \frac{\partial}{\partial x_j}(-\overline{\rho u_i'' u_j''}) \quad\dots\dots\dots(2)$$

$$\frac{\partial \bar{\rho}\tilde{h}}{\partial t} + \frac{\partial \bar{\rho}\tilde{u}_i \tilde{h}}{\partial x_i} = \frac{\partial}{\partial x_i}\left(\frac{\mu_t}{\sigma_h}\frac{\partial \tilde{h}}{\partial x_i}\right) + \tilde{S}_h \quad\dots\dots(3)$$

where t, x_i, $\tilde{u}_i$ and u_i'' respectively represent time, Cartesian coordinates and Favre-averaged and fluctuating velocity component. The notations, μ, $\bar{\rho}$, $\bar{p}$ and $\bar{h}$, are viscosity, time-averaged density and pressure and Favre-averaged specific enthalpy. $\tilde{S}_h$ represents the source term due to chemical reaction and radiation. The turbulent Prandtl number for enthalpy, σ_h, is put equal to 0.7. The Favre-averaged turbulent kinetic energy ($\tilde{k}$) and its dissipation rate ($\tilde{\varepsilon}$) are described by the standard $\tilde{k}$–$\tilde{\varepsilon}$ model[7] as,

$$\frac{\partial \bar{\rho}\tilde{k}}{\partial t} + \frac{\partial \bar{\rho}\tilde{u}_i \tilde{k}}{\partial x_i} = \frac{\partial}{\partial x_i}\left[\left(\mu + \frac{\mu_t}{\sigma_k}\right)\frac{\partial \tilde{k}}{\partial x_i}\right]$$

$$-\overline{\rho u_i'' u_j''}\frac{\partial \tilde{u}_j}{\partial x_i} + \beta g_i \frac{\mu_t}{\text{Pr}_t}\frac{\partial \tilde{T}}{\partial x_i} - \bar{\rho}\tilde{\varepsilon} \quad\dots\dots(4)$$

$$\frac{\partial \bar{\rho}\tilde{\varepsilon}}{\partial t} + \frac{\partial \bar{\rho}\tilde{u}_i \tilde{\varepsilon}}{\partial x_i} = \frac{\partial}{\partial x_i}\left[\left(\mu + \frac{\mu_t}{\sigma_\varepsilon}\right)\frac{\partial \tilde{\varepsilon}}{\partial x_i}\right] - C_{2\varepsilon}\bar{\rho}\frac{\tilde{\varepsilon}^2}{\tilde{k}}$$

$$+C_{1\varepsilon}\frac{\tilde{\varepsilon}}{\tilde{k}}\left[-\overline{\rho u_i'' u_j''}\frac{\partial \tilde{u}_j}{\partial x_i} + (1-C_{3\varepsilon})\beta g_i \frac{\mu_t}{\text{Pr}_t}\frac{\partial \tilde{T}}{\partial x_i}\right] \quad\dots(5)$$

The notations, $\tilde{T}$, μ_t $(=\bar{\rho}C_\mu(\tilde{k}^2/\tilde{\varepsilon}))$, β, g_i and Pr_t, are Favre-averaged temperature, turbulent viscosity, thermal expansion coefficient, gravity and turbulent Prandtl number for $\tilde{k}$. The model constants have the following values.

$$C_{1\varepsilon}=1.44, \ C_{2\varepsilon}=1.92, \ C_\mu=0.09,$$
$$\sigma_k=1.0, \ \sigma_\varepsilon=1.3, \ \text{Pr}_t=0.85$$

2.2. Turbulent Combustion Model

The mixture fraction/assumed pdf approach[8] is based on infinitely fast chemistry with the instantaneous thermochemical state of the fluid given as a function of the mixture fraction. The mixture fraction, f, is defined as

$$f = \frac{Z_k - Z_{kO}}{Z_{kF} - Z_{kO}} \quad\dots\dots\dots(6)$$

where Z_k is the mass fraction of the k-th element. The subscript, O, denotes a value at the inlet of the oxidizer stream and the subscript, F, denotes a value at the inlet of the fuel stream. The conservation equations for the Favre-averaged mean and variance of the mixture fraction, $\tilde{f}$ and $\tilde{f}''^2$ are given as

$$\frac{\partial \bar{\rho}\tilde{f}}{\partial t} + \frac{\partial \bar{\rho}\tilde{u}_i \tilde{f}}{\partial x_i} = \frac{\partial}{\partial x_i}\left(\frac{\mu_t}{\sigma_t}\frac{\partial \tilde{f}}{\partial x_i}\right) \quad\dots\dots\dots(7)$$

$$\frac{\partial \bar{\rho}\tilde{f}''^2}{\partial t} + \frac{\partial \bar{\rho}\tilde{u}_i \tilde{f}''^2}{\partial x_i} = \frac{\partial}{\partial x_i}\left(\frac{\mu_t}{\sigma_t}\frac{\partial \tilde{f}''^2}{\partial x_i}\right)$$

$$+C_g \mu_t \left(\frac{\partial \tilde{f}}{\partial x_i}\right)^2 - C_d \bar{\rho}\frac{\tilde{k}}{\tilde{\varepsilon}}\tilde{f}''^2 \quad\dots\dots\dots(8)$$

where the constants have the following values.

$$\sigma_t=0.7, \ C_g=2.86, \ C_d=2.0$$

The pdf for the conserved scalar, f, is introduced to consider the effects of turbulent fluctuation. The Favre pdf is defined as

$$\tilde{p}(f) = \frac{\rho^e(f)}{\bar{\rho}}p(f) \quad\dots\dots\dots\dots(9)$$

where $\rho^e(f)$ is the density at the equilibrium state.
The Favre-averaged species mole fractions and temperature in an adiabatic system can be computed as

$$\tilde{\phi} = \int_0^1 \tilde{p}(f)\phi(f)df. \quad\dots\dots\dots(10)$$

The Favre pdf, $\tilde{p}(f)$, is assumed to have the profile of the β-function.[8]

2.3. Radiative Heat Transfer

The finite volume method[9,10] is adopted to model radiative heat transfer in the furnace. It solves the following radiative transfer equation for a finite number of radiation intensities, each associated with the direction vector, $\mathbf{s}$.

$$(\mathbf{s}\cdot\nabla)\overline{I(\mathbf{r},\mathbf{s})} = -\bar{\kappa}\overline{I(\mathbf{r},\mathbf{s})} + \bar{\kappa}\overline{I_b(\mathbf{r})} \quad\dots\dots\dots(11)$$

$\overline{I(\mathbf{r},\mathbf{s})}$ represents the time-averaged radiation intensity in the direction, $\mathbf{s}$, at the position, $\mathbf{r}$. $\overline{I_b(\mathbf{r})}$ is the time-averaged blackbody radiation intensity of the gas medium. The polar and azimuthal angles are uniformly subdivided into N_θ and N_ϕ respectively with the total of $N_\theta \times N_\phi$ control angles for the 4π steradian solid angle. Here N_θ is equal to 4 and N_ϕ is equal to 8 with 32 discretized angular components of the radiation intensity. The absorption coefficient, $\tilde{\kappa}$, is obtained by the weighted-sum-of-gray-gases model[11] as a mixture of CO, CO_2 and H_2O. It is a reasonable compromise between the simple gray gas assumption and the band models that take into account particular absorption bands.

2.4. Conduction and Convection Heat Transfer

Conduction heat transfer in a slab is described by the following transient two-dimensional Fourier equation,

$$\frac{\partial}{\partial x}\left(k_s \frac{\partial T_s}{\partial x}\right) + \frac{\partial}{\partial y}\left(k_s \frac{\partial T_s}{\partial y}\right) = \rho_s C_{p,s}\frac{\partial T_s}{\partial t} \quad\dots\dots(12)$$

where T_s, k_s, ρ_s and $C_{p,s}$ are the temperature, temperature-dependent thermal conductivity, density and specific heat of the slab. Conduction in the direction that the slab moves is ignored as negligible. The convective heat transfer coefficient to cooling water in the skid pipe is given from the Dittus–Boelter correlation for fully developed turbulent pipe flow as,
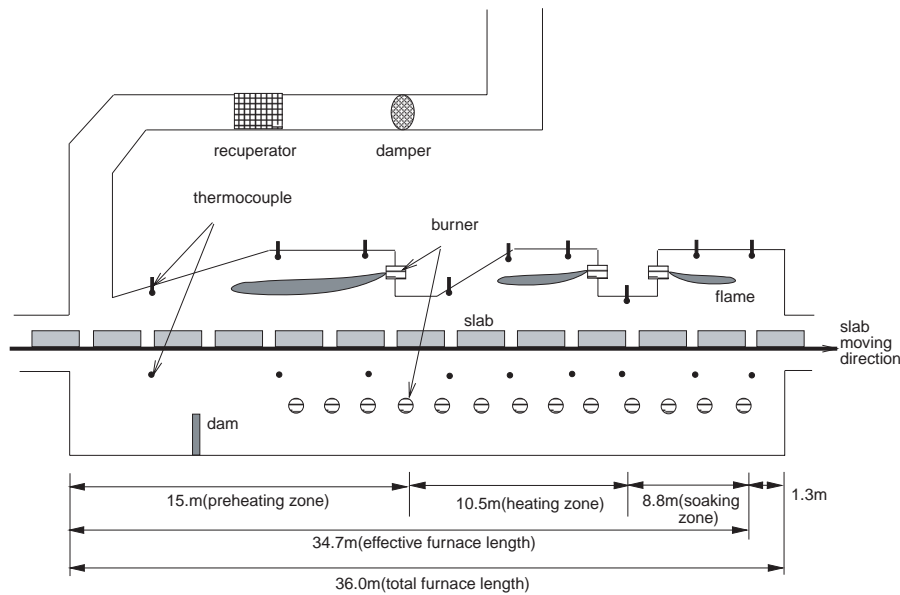
Fig. 1. Layout of the re-heating furnace.

Table 1. Composition of the mixed gas.

Species	Volume fraction(%)
H_2	35.94
N_2	23.84
O_2	0.41
CO	12.17
CH_4	15.39
C_2H_4	1.11
C_2H_6	0.23
CO_2	10.91

Table 2. Fuel flow rates at 273 K and 1 atm.

		Preheating zone	Heating zone	Soaking zone	Sum
Upper zone	Fuel flow rate (km^3/hr)	4.50 (22.6 %)	3.80 (19.0 %)	1.46 (7.3 %)	9.76 (48.9 %)
Lower zone	Fuel flow rate (km^3/hr)	4.59 (23.0 %)	3.94 (19.8 %)	1.65 (8.3 %)	10.18 (51.1 %)
Total fuel flow rate (km^3/hr)		9.09 (45.6)	7.74 (38.8 %)	3.11 (15.6 %)	19.94 (100 %)

$$Nu = 0.23Re^{0.8}Pr^{0.33} \quad \dots\dots\dots\dots\dots\dots(13)$$

where Nu, Re and Pr are the Nusselt, Reynolds and Prandtl number in the skid pipe.

3. Results and Discussion

3.1. Specifications of the Furnace

The layout in **Fig. 1** is for a walking beam type of a re-heating furnace in the No. 2 hot strip mill in POSCO. It has the dimension of $36\,m \times 10.7\,m \times 5.2\,m$ with axial flow burners in the upper zone and side flow burners in the lower zone. The mixed gas used as fuel has a lower heating value of $11\,723\,KJ/m^3$ at 273 K and 1 atm. The composition of the mixed gas is given in **Table 1**. The total fuel flow rate is $19.94\,km^3$/hr at 273 K with the fuel flow rate in each zone given in **Table 2**. The total air flow rate is $171.54\,km^3$/hr at 768 K and given as proportional to the fuel flow rate in each
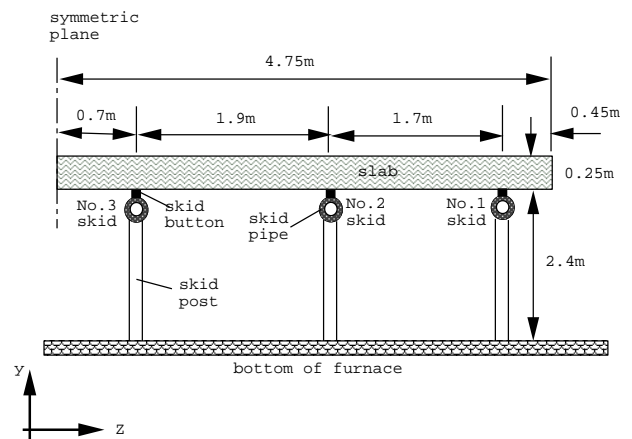

Fig. 2. Layout of the slab with skid support.

zone. The overall equivalence ratio is 0.909, which is fuel-lean combustion with 10 percent of excess air.

The furnace may be divided into three distinct zones along the direction that slabs move—preheating, heating and soaking zone. Slabs move in the opposite direction to the primary flow of combustion product gas in an uptake type furnace. The skid system to support slabs in **Fig. 2** distorts the heat flux by providing conduction paths between the slab and coolant in the skid pipe. The skid system and other structural components in the lower zone block thermal radiation from burner flames. It is of critical importance to accurately determine the overall heat transfer coefficient to the slabs in the current practice of monitoring operation[12] and analysis of the furnace. The slabs here are composed of low carbon steel (carbon mass fraction: 0.06–0.27%) while the skid buttons are composed of the stainless steel, STPT38.[13]

3.2. Simulation of the Furnace

Steady state calculation is performed for a half domain of the furnace with the symmetric boundary condition for all variables on the central plane. The computational grid
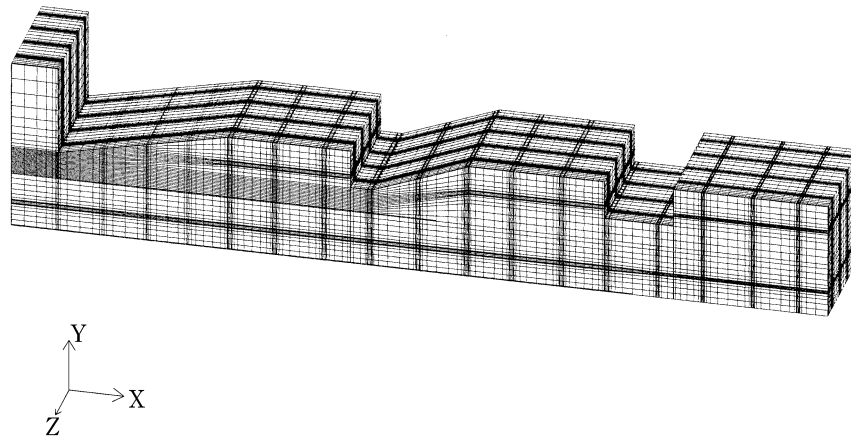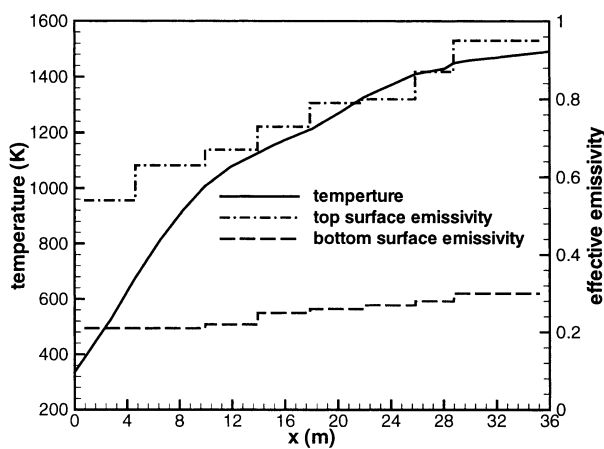
Fig. 3. Computational grid of the re-heating furnace.

Fig. 4. Typical profiles of the temperature and effective emissivity on the slabs in the axial direction of the furnace (x: axial position from the entrance).

Fig. 5. Diagram of the global energy flow.

for the furnace in **Fig. 3** has activated cells of about 440 000. The constant pressure of 20 Pa gauge is applied at the stack through which exhaust gas leaves to the recuperator. The profiles of the temperature and effective emissivity in **Fig. 4** are used as the boundary condition for radiative heat transfer on the slab. The effective emissivity was defined to be the emissivity of the slab taking into account the effects of the surface condition, the material type and shielding by the surrounding structural components, *etc*. The effective emissivity on the top surface of a slab increases progressively as the surface becomes oxidized at a high ambient temperature. The effective emissivity on the bottom surface is lower than that on the top surface because of the structures such as the skid beams, walking beams and posts shielding radiation from burner flames. As radiation is the dominant heat transfer mode, the overall heat transfer coefficient is roughly proportional to the effective emissivity on the slab surface.[12] The furnace is bounded by refractory walls, the emissivity of which is set equal to 0.75.

Figure 5 shows the energy flow diagram with comparison between predictions and measurements. The amounts of energy supplied by fuel and air and heat loss through the walls are specified as boundary conditions for the burners and furnace walls. The total input energy is composed of
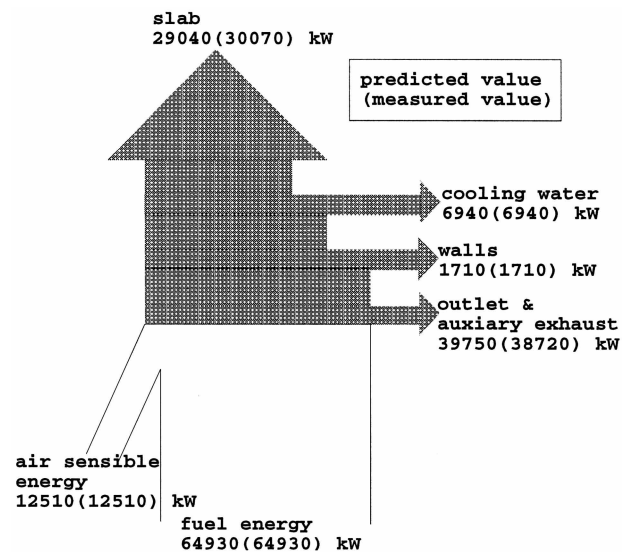
the fuel energy of 64 930 kW and the sensible energy of air of 12 510 kW. The predicted heat transfer rate to the slabs is 29 040 kW which corresponds to 37.5 % of the total input energy. This is slightly lower than the measured heating efficiency of 38.8 %. The heat transfer by radiation amounts to 93.6 % of the total heat transferred to the slabs. As the furnace temperature increases, the radiative heat flux which is proportional to ΔT^4 increases much more rapidly than the convective heat flux.

Figures 6(a) and **6(b)** show temperature distributions on vertical cross sections in the furnace. The former is through the axial flow burners next to the symmetric plane, while the latter is through the axial flow burners next to the side wall in the upper zone. Figures 6(c) and 6(d) show the temperature distributions on horizontal cross sections. The former is through the axial flow burners in the upper zone, while the latter is through the side flow burners in the lower zone. Note that the flames are the longest in the preheating zone due to the largest fuel flow rates. On the other hand those in the soaking zone are the shortest due to the smallest fuel flow rates. The flames next to the symmetric plane look longer than those next to the side wall in the upper zone in Figs. 6(a) and 6(b). It is because the flames next to the side wall are deflected by the upward flow through the
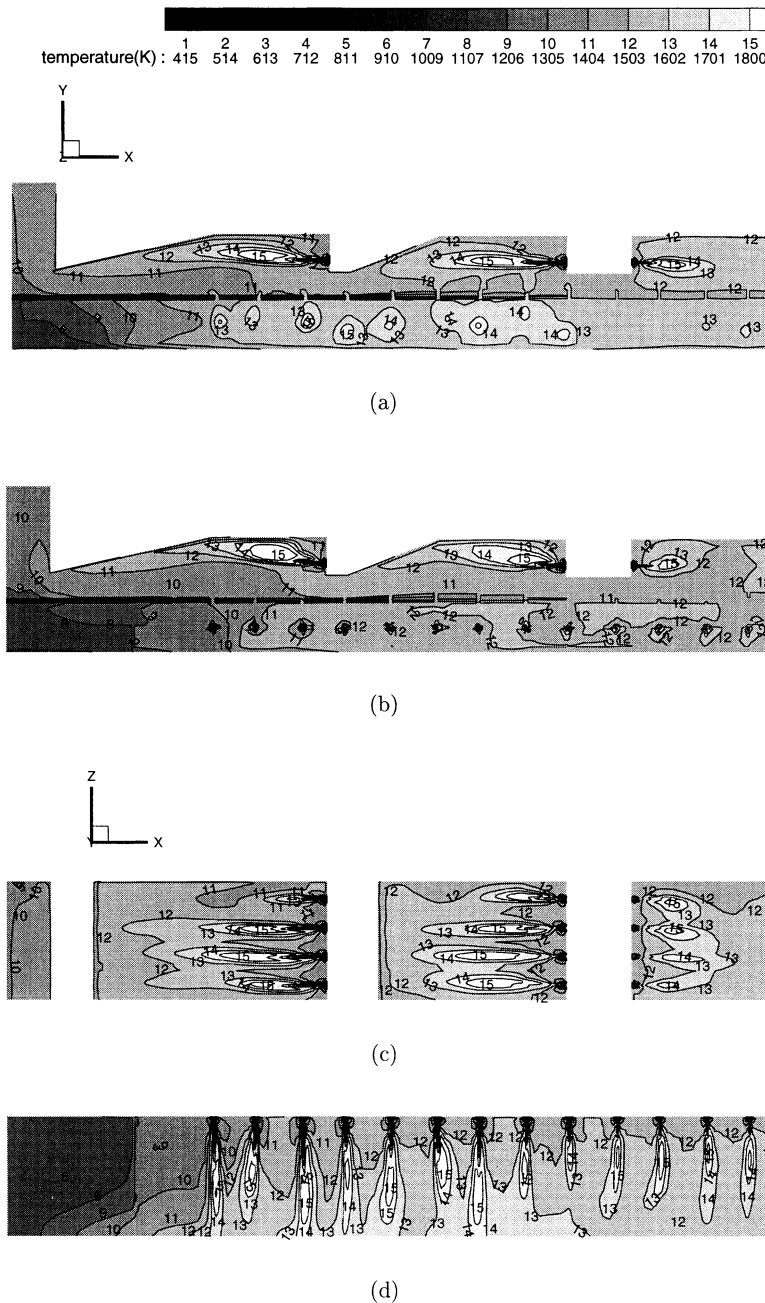
temperature(K) :

	1	2	3	4	5	6	7	8	9	10	11	12	13	14	15
	415	514	613	712	811	910	1009	1107	1206	1305	1404	1503	1602	1701	1800

(a)

(b)

(c)

(d)

Fig. 6. Predicted distribution of the temperature in the furnace.

gap between the furnace wall and slabs. Results show that the temperature distribution in the furnace is a combined effect of the complicated three-dimensional flow and flame configurations and the boundary conditions in the given furnace geometry.

Figure 7 shows axial distributions of the predicted heat flux on the top and bottom surface of the slabs. Note that the heat flux in the preheating and heating zone is larger than that in the soaking zone. The heat flux on the top surface drops at the nose regions that are located away from the burner flames. **Table 3** lists the calculated heat transfer rates on the top and bottom surface of the slabs in each zone. The predicted heat transfer rate on the top surface is 19 880 kW, which is 68.5 % of the total heat transfer to the slabs. The rest through the bottom surface is lower than that due to a lower effective emissivity on the bottom surface. The predicted heat transfer rates in the preheating, heating
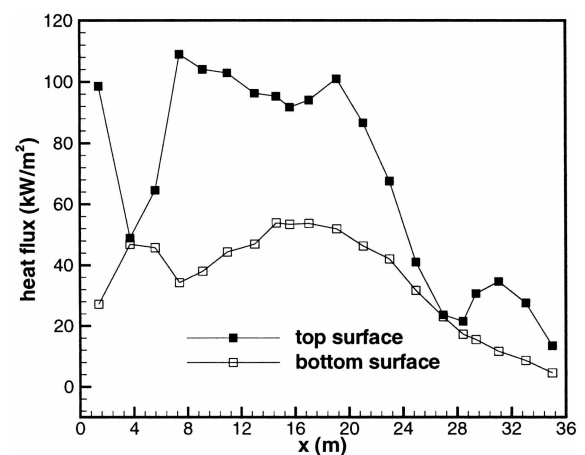

Fig. 7. Predicted heat fluxes on the top and bottom surface of the slab along the axial direction of the furnace (x: axial position from the entrance).

Table 3. Calculated heat transfer rates to the slabs.

		Preheating zone	Heating zone	Soaking zone	Sum
Top surface	Radiative heat transfer rate (kW)	10,200	6,820	2,090	19,110
	Convective heat transfer rate (kW)	580	170	20	770
	Total heat transfer rate (kW)	10,780 (37.1 %)	6,990 (24.1 %)	2,110 (7.3 %)	19,880 (68.5 %)
Bottom surface	Radiative heat transfer rate (kW)	3,800	3,350	920	8,070
	Convective heat transfer rate (kW)	720	320	50	1,090
	Total heat transfer rate (kW)	4,520 (15.6 %)	3,670 (12.6 %)	970 (3.3 %)	9,160 (31.5 %)
Sum	Radiative heat transfer rate (kW)	14,000	10,170	3,010	27,180
	Convective heat transfer rate (kW)	1,300	490	70	1,860
	Total heat transfer rate (kW)	15,300 (52.7 %)	10,660 (36.7 %)	3,080 (10.6 %)	29,040 (100 %)

and soaking zone amount to 52.7%, 36.7% and 10.6% of the total heat transfer to the slabs.

Figures 8 and **9** show the predicted heat fluxes on the top and bottom surface of the slabs at different axial locations. The z coordinate is the distance in the normal direction from the symmetric plane. The heat flux on the top surface is relatively uniform at all axial locations in Fig. 8. It is because the flames of the axial flow burners are aligned in a parallel direction in the upper zone as shown in Fig. 6. The non-uniform heat flux on the bottom surface in Fig. 9 is related with the non-uniform temperature distribution in the lower zone in Fig. 6. Longer flames from the side flow burners in the preheating and heating zone result in the peak heat flux near the symmetric plane while shorter flames in the soaking zone result in more uniform distribution of the heat flux.

3.3. Conduction Calculation in the Slab

The computational grid in **Fig. 10** is on a cross sectional plane of the slab with activated cells of about 2 400. Conduction in the direction normal to the cross sectional plane is ignored as negligible. The boundary conditions on the slab and skid system are shown in **Fig. 11**. The contact resistance between the slab and the skid button is given as a function of the contact temperature by the experimental correlation of Howells et al.[14] The convective heat transfer coefficient in the skid pipe is 1248 W/m²K according to Eq. (13). The temperature of cooling water in the skid pipe is assumed to have a constant value of 315 K. The initial temperature of the skid button is 606 K and the initial temperature of the slab is 335 K. The heat flux on the slab is scaled up to match the heating efficiency of the furnace from 37.5% to 38.8% as given in Fig. 5.

Figure 12 shows the predicted axial variations of the mean slab temperature and the mean temperatures on the top and bottom surface of the slab. Note the discrepancy between the applied boundary condition and the resulting mean surface temperature of the slab in Fig. 12. It would require excessive computational burden to go through an it-
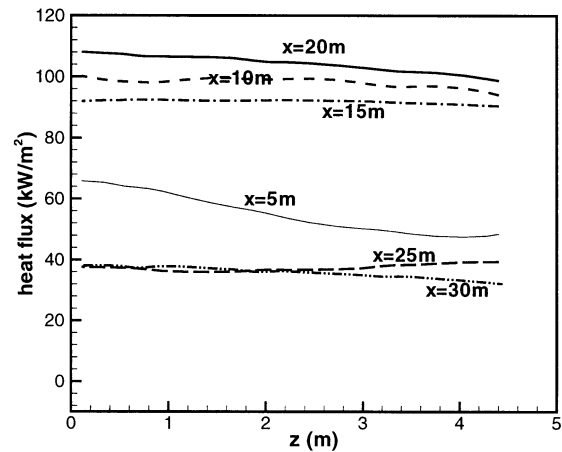

Fig. 8. Predicted heat fluxes on the top surface along the length direction of the slab (x: axial position from the entrance, z: distance from the symmetric plane).
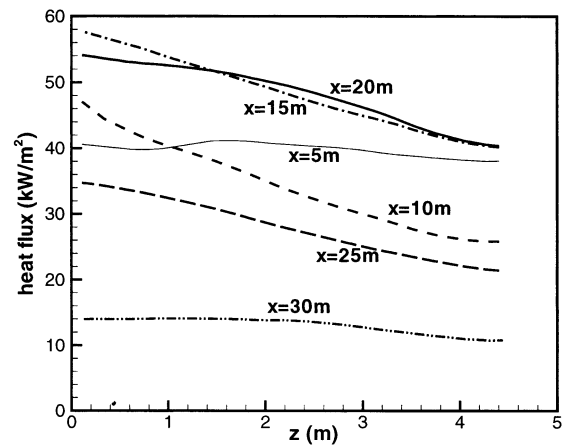

Fig. 9. Predicted heat fluxes on the bottom surface along the length direction of the slab (x: axial position from the entrance, z: distance from the symmetric plane).

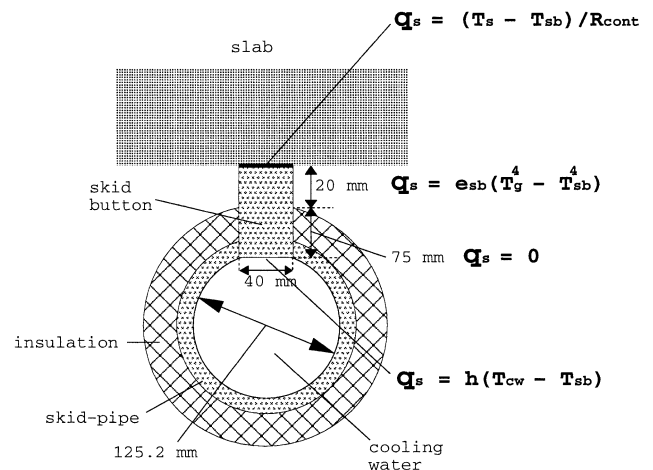Fig. 10. Computational grid of the slab with skid buttons.

Fig. 11. Boundary conditions for conduction calculation of the slab including the skid button (e_{sb}: emissivity of skid button).
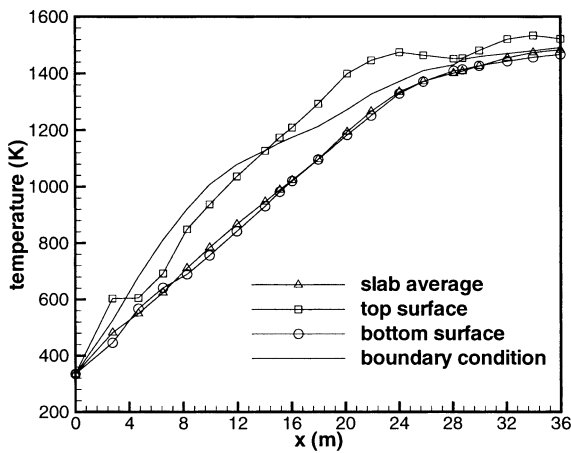
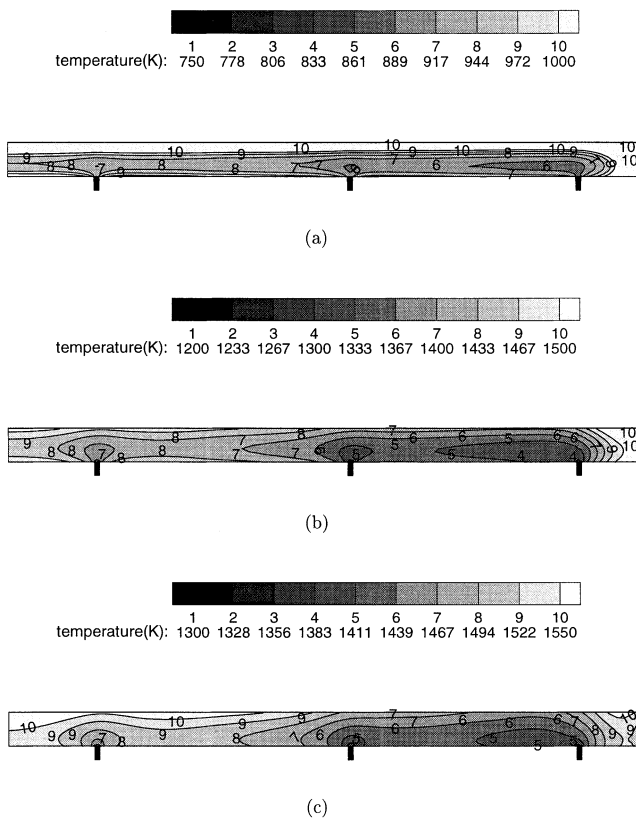**Fig. 12.** Predicted temperatures of the slab along the axis of the furnace (x: axial position from the entrance).

(a)

(b)

(c)

Fig. 13. Predicted distribution of the slab temperature at the exit of each zone; (a) preheating zone (b) heating zone (c) soaking zone.

Fig. 14. Different shapes of the skid button under consideration.

In Fig. 13(c) the local minimum temperature occurs on the bottom surface between No. 1 and No. 2 skids. It is because of a lower effective emissivity on the bottom surface and a higher mean slab temperature in the soaking zone. Here the non-uniform slab temperature is primarily due to the non-uniform heat flux from side flow burners as shown in Fig. 9. The edge region has a higher temperature due to additional radiative exposure through the side area of the slab. The calculated mean slab temperatures at the end of the preheating, heating and soaking zone are 989 K, 1 401 K and 1 483 K. The increases in the mean slab temperature through the preheating, heating and soaking zone are 654 K, 412 K and 82 K respectively.

3.4. Parametric Study on Skid Mark Severity

Parametric study is performed on skid mark severity with respect to the length and shape of the skid button and the convective heat transfer coefficient in the skid pipe. Skid mark severity is defined here as the difference between the mean temperature on the bottom surface and the average temperature at the contact regions between the slab and the skid buttons. Skid mark severity represents the degree of non-uniform temperature distribution due to conduction heat loss from the slab to the skid system. The effects of the non-uniform heat flux from side flow burners, which has turned out to be another major factor, are not taken into account in this parametric study.

Various different shapes of the skid button are shown in **Figs. 14(a)–14(d)**. They all have the same height and the same contact area between the slab and the skid buttons. The shape in Fig. 14(a) is the one actually installed in the furnace under consideration. The distributions of the slab temperature in **Figs. 15(a)–15(c)** correspond to the shapes of the skid button in Figs. 14(b), 14(c) and 14(d). The results for the skid button in Fig. 14(a) are in Fig. 13(c). The skid mark severities in **Fig. 16** also match the cases in Fig. 14. The mean slab temperatures for Figs. 14(a), 14(b), 14(c) and 14(d) are 1 483 K, 1 452 K, 1 484 K and 1 485 K, while the skid mark severities for the same cases are 73 K, 204 K, 72 K and 55 K respectively. The mean temperatures of the skid button in Figs. 14(a), 14(b), 14(c) and 14(d) are 787 K, 521 K, 853 K and 915 K respectively. The skid button in

erative procedure between the furnace and slab calculations to reduce the gap in Fig. 12. The temperature difference between the top and bottom surface increases in the preheating and heating zone while it decreases in the soaking zone. It has the maximum value of 216 K in the heating zone while it decreases to 55 K at the furnace exit. The mean slab temperature and the mean temperature on the bottom surface are close to each other due to a lower heat flux on the bottom surface.

Figures 13(a)–13(c) show distributions of the slab temperature on the cross sectional planes at the end of the preheating, heating and soaking zone. The local minimum temperature occurs inside the slab in Figs. 13(a) and 13(b).
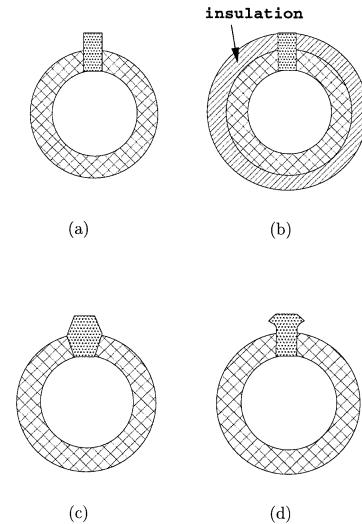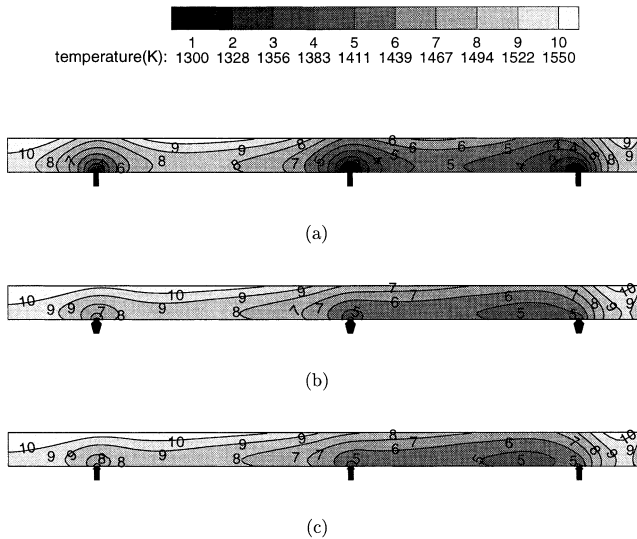
Fig. 15. Distributions of the slab temperature at the exit of the furnace for different shapes of the skid button; (a) for Fig. 14(b), (b) for Fig. 14(c), (c) for Fig 14(d).
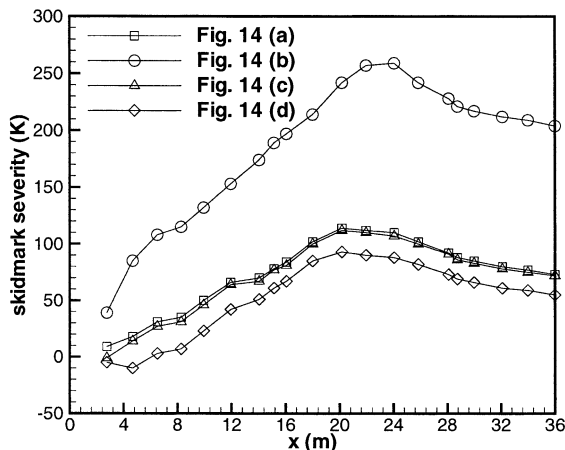

Fig. 16. Skid mark severity along the axis for different shapes of the skid button in Fig. 14 (x: axial position from the entrance).

Fig. 17. Distributions of the slab temperature at the exit of the furnace for different heights of the skid button; (a) 5 mm, (b) 10 mm, (c) 30 mm, (d) 40 mm.

Fig. 18. Skid mark severity along the axis for different heights of the skid button (x: axial position from the entrance).

Fig. 14(b) results in the highest skid mark severity and the lowest mean slab and skid button temperature. The skid button in Fig. 14(d) results in the lowest skid mark severity and the highest mean slab and skid button temperature. The skid button in Fig. 14(b) has no radiative exposure area, while the skid button in Fig. 14(d) has the largest exposure area, that is, the area above the insulation of the skid pipe in Fig. 11.

Distributions of the slab temperature are shown with respect to the height of the skid button in **Fig. 17**, which is the height above the insulation of the skid pipe in Fig. 11. The heights of the skid button for Figs. 17(a), 17(b), 17(c) and 17(d) are 5 mm, 10 mm, 30 mm and 40 mm respectively. The skid mark severities in **Fig. 18** match the cases in Fig. 17. The mean slab temperatures in Figs. 17(a), 17(b), 17(c) and 17(d) are 1 459 K, 1 471 K, 1 490 K and 1 494 K, while the skid mark severities for the same cases are 170 K, 110 K, 50 K and 34 K. The mean temperatures of the skid button in Figs. 17(a), 17(b), 17(c) and 17(d) are 588 K, 625 K, 930 K and 1 002 K respectively. These results show
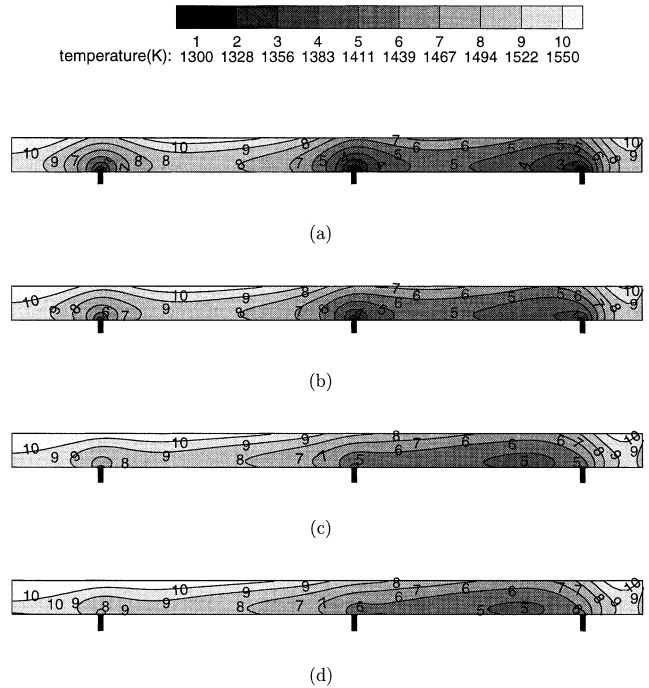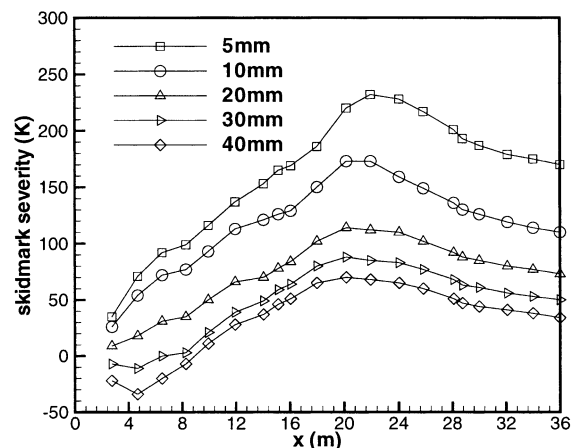
lower skid mark severity with less conduction heat loss to the skid system for the case with a larger radiative exposure area as in Fig. 16. The total heat transferred to the coolant is composed of the heat conducted from the slab and the heat transferred by radiation to the skid button, with the latter dominant over the former in all cases in Fig. 15 and 17.

Distributions of the slab temperature are shown with respect to the convective heat transfer coefficient in the skid pipe in **Fig. 19**. The convective heat transfer coefficients in Figs. 19(a), 19(b) and Fig. 13(c) are 670, 2 345 and 1 248 W/m²K respectively. The skid mark severities in **Fig. 20** match the cases in Fig. 19. The mean slab temperatures at the exit of the furnace for Figs. 19(a), 19(b) and Fig. 13(c) are 1 484 K, 1 480 K and 1 483 K, while the skid mark severities for the same cases are 58 K, 84 K and 73 K. The mean temperatures of the skid button in Figs. 19(a), 19(b) and Fig. 3(c) are 909 K, 705 K and 787 K respectively. Skid
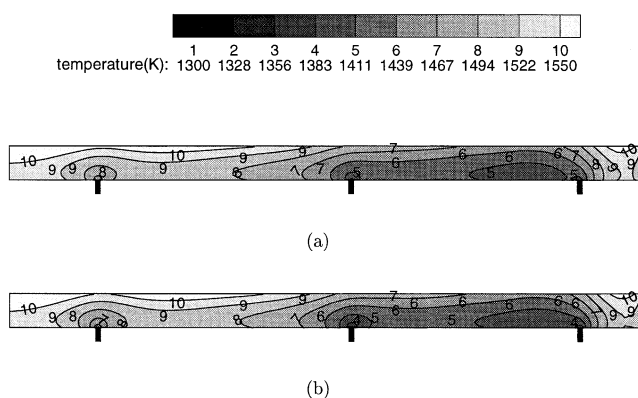
temperature(K):
1 1300 2 1328 3 1356 4 1383 5 1411 6 1439 7 1467 8 1494 9 1522 10 1550

(a)

(b)

Fig. 19. Distributions of the slab temperature at the exit of the furnace for different convective heat transfer coefficients in the skid pipe; (a) 670 W/m² K, (b) 2345 W/m² K.
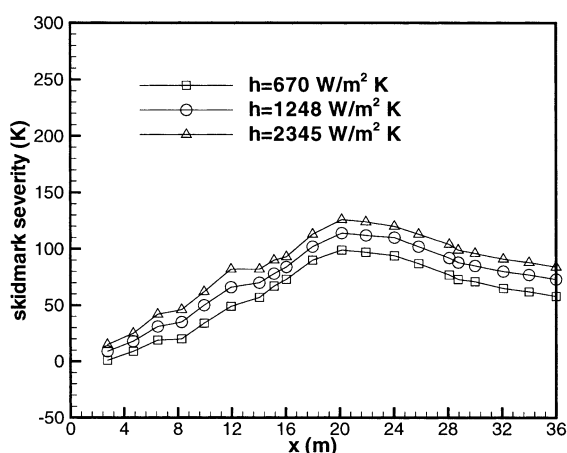

Fig. 20. Skid mark severity along the axis for different convective heat transfer coefficients in the skid pipe (x: axial position from the entrance).

mark severity decreases as the convective heat transfer coefficient decreases with reduced heat loss from the slab. It may be said that the radiative exposure area on the skid button has a dominant effect on skid mark severity over the convective heat transfer coefficient in the skid pipe.

4. Conclusions

Following conclusions could be drawn from heat transfer analysis of the slabs in a walking beam type of a reheating furnace in POSCO. Although the numerical results are for the specific example under consideration, the same methodology may be applied to any similar problems of re-heating furnaces in the design phase or currently in operation.

(1) The fraction of the total energy transferred to slabs may be interpreted as the heating efficiency of the furnace. It is calculated as 37.5%, which is in good agreement with the measurement of 38.8%. Most heat transfer to slabs occurs by radiation in the preheating and heating zone due to higher fuel flow rates and lower slab temperatures. The fraction of the heat transfer through the top surface of slabs

is 68.5%, which is larger than that through the bottom surface due to shielding by the surrounding skid structures.

(2) Non-uniform temperature distribution in the slab results from the non-uniform heat flux in the lower preheating and heating zone and the conduction heat loss to the skid system. According to the calculation results the local minimum temperature occurs inside the slab in the preheating and heating zone. The non-uniform heat flux from side flow burners turns out to be of significant importance in the slab temperature distribution. In the soaking zone the local minimum temperature occurs on the bottom surface of the slab between the No. 1 and No. 2 skids. It is due to a lower effective emissivity on the bottom surface and a higher mean slab temperature in the soaking zone.

(3) Parametric study is performed for skid mark severity with respect to the length and shape of the skid button and the convective heat transfer coefficient in the skid pipe. Although a larger exposure area of the skid button increases the total heat transferred to the coolant, it reduces conduction heat loss from the slab to result in a lower skid mark severity. Skid mark severity also decreases as the convective heat transfer coefficient to the coolant decreases. Calculation results show that the radiative exposure area on the skid button has a dominant effect on skid mark severity over the convective heat transfer coefficient in the skid pipe.

(4) Detailed calculation results in this paper may help to determine a more accurate overall heat transfer coefficient, which is of critical importance for the on-line simulator program currently used to monitor the slabs in terms of the temperatures measured at several representative locations in the furnace. The overall heat transfer coefficient to the slab is roughly proportional to the effective emissivity defined to consider the slab surface condition and shielding by the skid structures in the lower zone.

REFERENCES

1) R. Ford, N. V. Suryanarayana and J. H. Johnson: *Ironmaking Steelmaking*, **3** (1980), 140.
2) Zongyu Li, P. V. Barr and J. K. Brimacombe: *Can. Metall. Q.*, **27** (1988), No. 3 187.
3) H. C. Hottel and A. Sarofim: Radiative Transfer, McGraw-Hill, New York, (1967).
4) P. V. Barr: *Metall. Mater. Trans. B.*, **26B** (1995), 851.
5) J. G. Kim, K. Y. Huh and I. T. Kim: *Numer. Heat Transfer*, *Part A*, in press.
6) FLUENT 5 User's Guide, Fluent Inc., Lebanon, (1998).
7) J. O. Hinze: Turbulence, McGraw-Hill Publishing Co., New York, (1975).
8) P. A. Libby and F. A. Williams: Turbulent Reacting Flows, Academic Press Inc., London, (1994).
9) E. H. Chui and G. D. Raithby: *Numer. Heat Transfer*, *Part B*, **23** (1993), 269.
10) G. D. Raithby and E. H. Chui: *J. Heat Transfer*, **112** (1990), 415.
11) M. F. Modest: *J. Heat Transfer*, **113** (1991), 650
12) M. J. Lee, J. G. Kim and K. T. Kim: POSCO Technical Report, (1996).
13) K. T. Kim: POSCO Technical Report, (1996).
14) R. I. L. Howells, J. Ward and S. D. Probert: *J. Iron Steel Inst.*, **212** (1973), 193.